NUMERICAL SIMULATION OF GEYSERING CREATED BY AIR POCKET RELEASE IN AN UPSTREAM VERTICAL SHAFT

Leandro C. Pinto[a], **José G. Vasconcelos**[b], **Daniel A. Piccilli**[a], **Robson L. Pachaly**[b], **Liriane E. Bock**[a] **and Rutineia Tassi**[a]

[a]*Department of Sanitary and Environmental Engineering, Universidade Federal de Santa Maria, Santa Maria 97105-900, RS, Brazil, leandro.pinto@ufsm.br, https://www.ufsm.br*

[b]*Department of Civil and Environmental Engineering, Auburn University, Auburn, AL 36849-5337, USA jgv@auburn.edu, https://www.auburn.edu/*

Keywords: Urbain Drainage Systems, Computational Fluid Dynamics, Compressible Flow, Finite Volume Method.

Abstract. Over the past decade, the air-water interaction in pipes with rapid filling has been studied to understand its effect on the formation of geysering phenomena. Geysering phenomena involve the displacement of an air pocket that is pressurized inside a storm drainage system during extreme precipitation events. The entrapped air pocket can move rapidly and displace water in drainage structures, causing explosive release when the biphasic fluid reaches grade elevation. Previous experimental and numerical studies have attempted to investigate the mechanism of geyser formation, but have not considered a numerical study with a geometry in which the air pocket is released through the upstream end of the dropshaft vertical drainage system. The objective of the present work is to study geysering phenomena through numerical simulations by analyzing the pressure results over time and following the movement of the air pocket inside the pipe from the initial air chamber up to the release in the upstream vertical dropshaft. An upstream end geometry was implemented in the OpenFOAM Volume of Fluid model, and the results obtained were qualitatively compared with scaled geometry results from an experimental study. The presented results showed strong similarities when qualitatively compared with the experimental one. It is possible to observe the displacement of the air pocket on the vertical shaft up to the time of its release. When mesh refinement was imposed on the model, the maximum displacement of water in the vertical shaft was observed. Statistical analyzes demonstrate a tendency of convergence of the model as the mesh resolution increases, indicating the possibility of scaling the model to match the experimental setup.

1 INTRODUCTION

Rapid filling can occur during extreme precipitation events in urban drainage systems, causing normal operation problems (Wright et al., 2019). One significant damaging phenomenon is geysering, which occurs when air-pockets are pressurized by the rapid inflow, forming an air-water mixture that promotes explosive eruptions in the system dropshafts. Several studies have been dedicated to the release of air and water in a dropshaft, using numerical and experimental methods. Guo and Song (1991) were one of the first to describe geysering phenomena analytically and numerically, but considering a single-phase discharge condition. Vasconcelos and Wright (2011) developed a simplified numerical model and were able to represent the main features of the experimental setup configuration. Muller et al. (2017) present results for the experimental setup considering the air pocket releases and displacement of the water surface in the dropshaft. These results could serve as parameter calibrations for a future computational fluid dynamics (CFD) model.

In the present work, a new configuration setup is modeled, considering air releases from the upstream end instead of the intermediary system location, using the volume of fluid (VOF) methodology. The results of displacement and pressure signals are analyzed and qualitatively compared from a large-scale experimental apparatus tested by Allasia et al. (2023). The main goal of the present study is to verify the convergence of the spatial resolution of the mesh by comparing the main statistical parameters of the pressure field and the variations of the level of the free surface of the water.

2 METHODOLOGY

2.1 Governing Equations

The governing equations for conservation laws of mass, momentum, and energy can be written respectively as follows:

$$\frac{\partial \rho}{\partial t} + \boldsymbol{\nabla} \cdot (\rho \mathbf{U}) = 0,$$

$$\frac{\partial (\rho \mathbf{U})}{\partial t} + \boldsymbol{\nabla} \cdot (\rho \mathbf{U}\mathbf{U}) = -\boldsymbol{\nabla} p + \boldsymbol{\nabla} \cdot (\mu \boldsymbol{\nabla} \mathbf{U}) + \rho \mathbf{g} - S_U, \tag{1}$$

$$\frac{\partial (\rho C_p T)}{\partial t} + \boldsymbol{\nabla} \cdot (\rho \mathbf{U} C_p T) = \boldsymbol{\nabla} \cdot (k \boldsymbol{\nabla} T) + S_T,$$

where ρ is the density, $\mathbf{U}$ is the velocity field, p is the pressure field, μ is the dynamic viscosity, $\mathbf{g}$ is the gravitational acceleration vector, and S_U represents any additional source term in the motion. In the energy equation T represents the temperature of the mixture, C_p is the specific heat, k is the thermal conductivity, and S_T any additional source term.

In the VOF model, the surface interface between the immiscible fluids is tracked throughout the domain. The properties of the fluid mixture are determined by the volume fraction of each phase. Therefore, a transport equation is solved for volume fraction, which is given by

$$\frac{\partial \alpha}{\partial t} + \boldsymbol{\nabla} \cdot (\alpha \mathbf{U}) + \boldsymbol{\nabla} \cdot [\alpha(1-\alpha)U_r] = 0, \tag{2}$$

where α is the volume fraction of water, and U_r the compression velocity. After solving the Eq. 2, it is possible to calculate all the properties of the fluid for each phase.

To represent compressible flow problems, some additional equations of state are used. The air phase is modeled using the ideal gas equation

$$\rho_a = \frac{p}{R_a T}, \tag{3}$$

and an adiabatic perfect fluid model was used for the water phase

$$\rho_w = \rho_{0_w} \left(\frac{p + B}{p_0 + B} \right)^{1/n_T}. \tag{4}$$

In Eq. 3 and 4, R_a is the constant of the gas, ρ_a and ρ_w are the densities of air and water, respectively, $\rho_{0_w} = 1,000 \text{ kg/m}^3$ is the reference density of the water, p_0 is the reference pressure, B is a constant of the model, and n_T is the isentropic constant. The reference viscosity values $\mu_a = 1.84 \times 10^{-5} \text{ N} \cdot \text{s/m}^2$ and $\mu_w = 3.65 \times 10^{-4} \text{ N} \cdot \text{s/m}^2$ were also used.

2.2 Geometric configuration

The computational domain simulated in the present study is presented in Fig. 1.
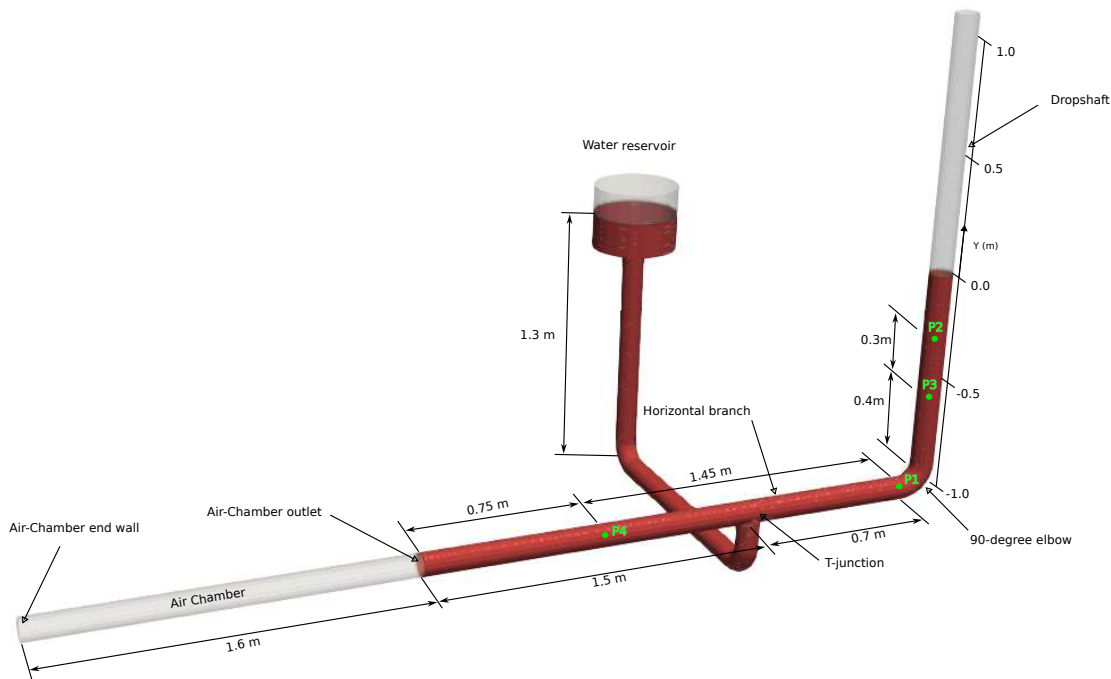
Figure 1: Computational domain for the flow problem simulated.

The system corresponds to a reduced geometric scale of the setup of Allasia et al. (2023), which is composed of pipes of diameter $D = 100$ mm. The horizontal branch, which is 2.2 m long, is coupled to an Air Chamber of 1.6 m long. At a distance of 1.5 m from the Air-Chamber outlet, a T-junction connection links the water reservoir that maintains the internal pressure of the system during air release. At the end of the horizontal branch, a vertical dropshaft that is 2 m long was connected through a 90-degree elbow. Since the T-junction connection to the water reservoir was positioned downward, the only path for air to escape is through the terminal dropshaft. Four probes were installed in the model to capture the pressure variations over time. Probes P4 and P1 were placed at distances of 0.75 m and 2.2 m from the Air-Chamber outlet in

the horizontal branch. Additional probes P2 and P3 were placed at distances 0.3 m and 0.6 m from the water surface level in dropshaft.

2.3 Numerical solution

The main governing equation must be solved using numerical methods. In the present study, the free open source software OpenFOAM (http://openfoam.org) was used, which consists of a free C++ library capable of numerically solving several physical problems. The *CompressibleInterFOAM* solver was specially designed to simulate nonisothermal immiscible flow fluids. The Finite Volume Method (FVM), based on the Pressure Implicit Split Operator (PISO), is used for the discretization of the previously presented governing equations. The adjusted time-step option was set to adapt the time step interval according to the maximum Courant number Co_{max} = 0.5. More details about the algorithm used in OpenFOAM can be found in Greenshields and Weller (2022).

As an initial condition, the fluid is hydrostatic, the system was filled to a predetermined piezometric head with the free surface positioned in the origin of the vertical coordinate Y as shown in Fig. 1. The beginning of the movement is imposed by the force of gravity acting at the air-water interface. Regarding the boundary conditions, a no-slip condition was imposed for the vector field **U** and *fixedFluxPressure* was applied for the scalar field p on all the walls of the pipe, including the end wall of the Air-Chamber. This boundary condition sets the pressure gradient according to the velocity boundary condition (http://openfoam.org). All other field variables were calculated on the basis of these main conditions. The k-ω SST model was used to give the closure of the governing equations. It is a commonly adopted turbulence model that combines the $k - \omega$ model near the wall with a $k - \epsilon$ model in the freestream (Menter, 1994).

The three-dimensional hexahedral mesh was generated using the software Salome (salome-platform.org), based on the geometric configuration shown in Fig. 1.
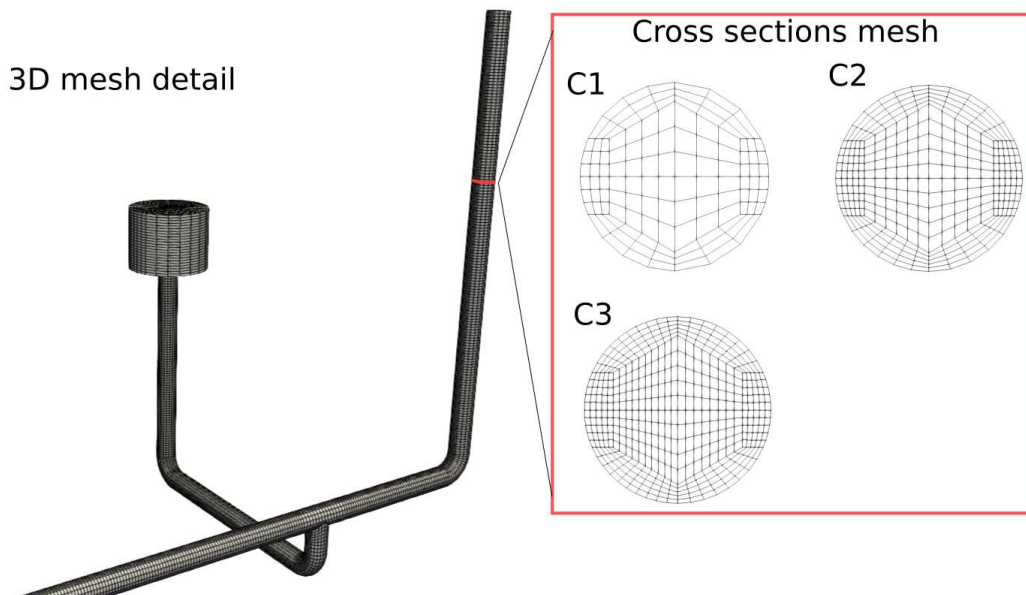
Figure 2: 3D mesh details showing the cross section resolutions for the cases C1, C2 and C3.

Three simulation cases have been conducted varying the mesh resolution (Fig. 2): C1 with a mesh of 92,512 cells and ≈ 13 cells per pipe diameter; C2 with a mesh of 380,050 cells and ≈ 20 cells per diameter and C3 with a mesh of 819,120 and ≈ 30 cells per diameter. Along the

longitudinal direction of the pipe, the resolutions for C1, C2, and C3 were, respectively, $\approx 8, 12$ and 18 cells per diameter. The reservoir was also meshed as can be observed in Fig. 2.

3 RESULTS AND DISCUSSION

When comparing the results for the probe pressure signals during time in Fig. 3, it is possible to observe that all cases presented very similar variations up to time ≈ 7.5. After this time, a high-frequency oscillation begins, and the pressure signals become different between the simulation cases.
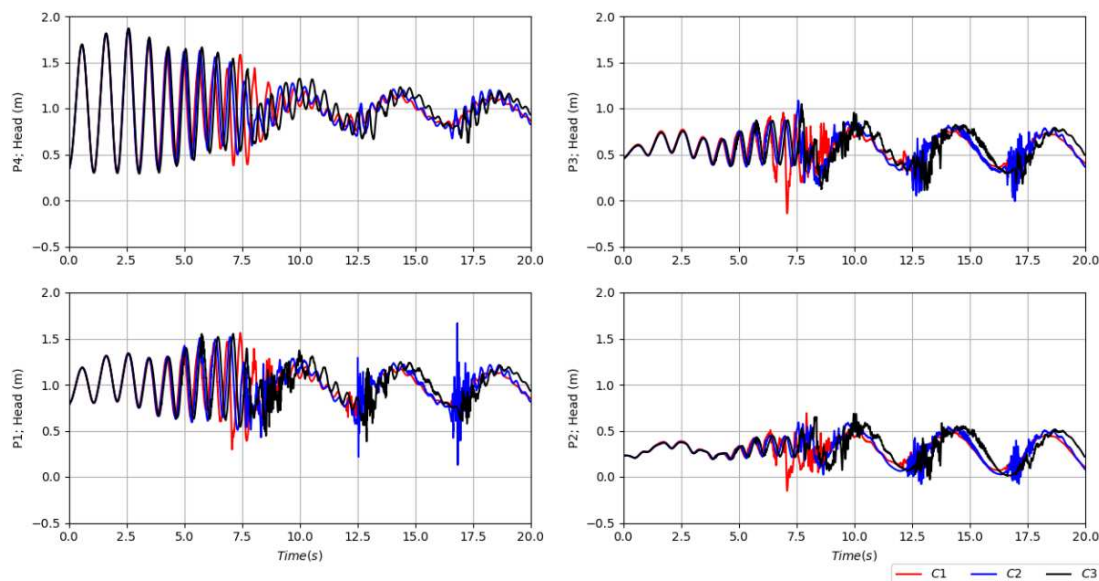
Figure 3: Pressure head results for each transducer for the cases C1, C2 and C3.

Probes P4 and P1, located in the horizontal branch, present a higher oscillation amplitude compared to the probes P3 and P2 installed in the dropshaft. This condition is caused by a possible oscillation of the water mass combined with the air-water interface in the air-chamber outlet. Similar pressure oscillations were also observed in experiments from Allasia et al. (2023), for the cases when the knife gate of the air-chamber was quickly opened.

The results of comparative pressure signal statistics, as shown in Fig. 3, are presented in Table 1. The values of the mean pressure head $\overline{p}/\gamma_w$ and the norm of the fluctuation of the pressure head $||p'/\gamma_w||$ are compared. In general, the results for case $C2$ are very close to those of the finest mesh in case $C3$.

When observing the air pocket displacement during the early stages of the geysering eruption in the dropshaft (Fig. 4) it is possible to observe that case $C1$ cannot well represent the same bubble advance compared to cases $C2$ and $C3$. The bubble does not touch the entire pipe wall and a maximum displacement of 0.2 m was observed for the free-surface water. On the other hand, case $C2$ could capture almost all physical geysering phenomena, including bubble displacement, trailing edge, and displacement of the free-surface water.

4 CONCLUSIONS

In this study, preliminary CFD simulation results for geysering created by an air pocket release in an end dropshaft pipe system, are presented. Three mesh resolutions were tested, and the middle resolution mesh case presented results similar to those of the highest mesh resolution

Probe	Case	$\overline{p}/\gamma_w$ (m)	$\overline{p}/\gamma_w$ Error (%)	$\|p'/\gamma_w\|$ (m)	$\|p'/\gamma_w\|$ Error (%)
P4	C1	0.973	1.72	0.102	33.44
	C2	0.961	0.41	0.136	11.61
	C3	0.957	-	0.154	-
P1	C1	0.970	1.67	0.124	29.62
	C2	0.953	0.10	0.179	1.39
	C3	0.954	-	0.176	-
P3	C1	0.550	3.94	0.123	27.40
	C2	0.521	1.56	0.170	0.88
	C3	0.530	-	0.169	-
P2	C1	0.281	1.91	0.116	24.27
	C2	0.261	5.25	0.156	1.58
	C3	0.275	-	0.154	-

Table 1: Results for pressure head statistics and comparative error between the cases simulated.
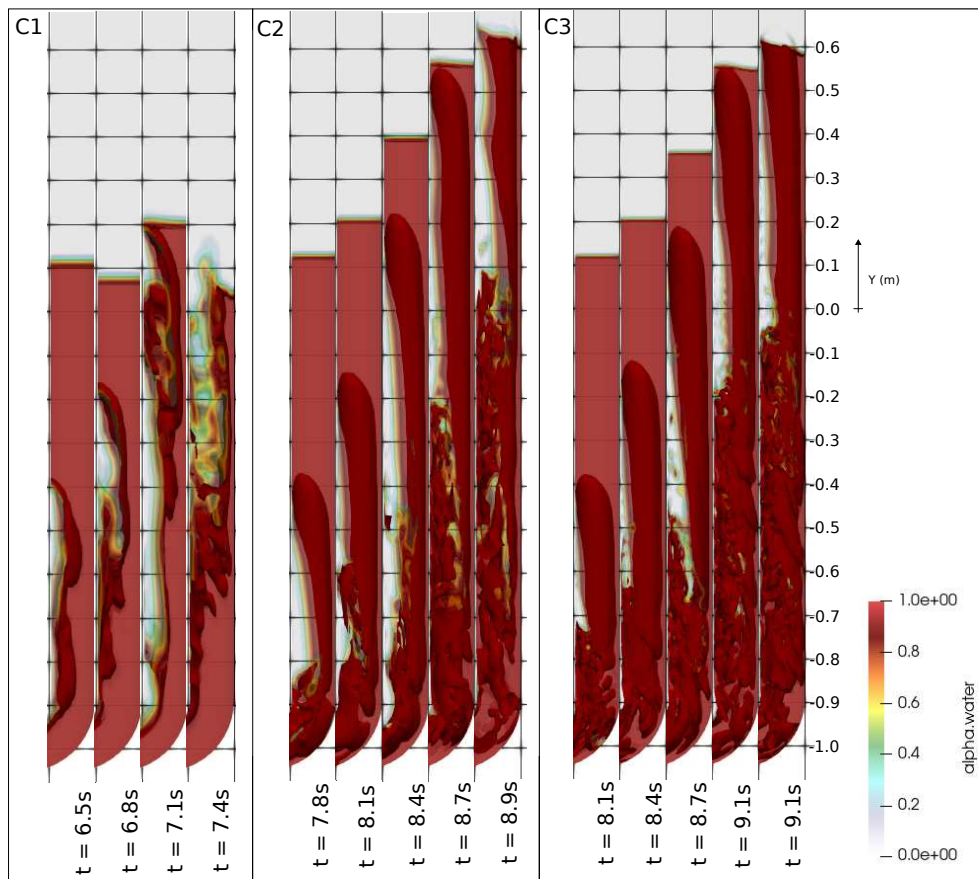
Figure 4: Air-pocket displacement visualization in the dropshaft for the cases C1, C2 and C3. The color scale pallet represents the water volume fraction α.

case. Such results demonstrate a tendency toward a possible convergence of the model when applied for the real-scale experimental setup. Besides the lack of possibility of comparing the simulation results with the experimental real scale from Allasia et al. (2023), it is important to note that similar pressure oscillations and displacement of the free surface in the dropshaft were observed here. Promising results can be expected when real-scale experimental tests can

be conducted.

ACKNOWLEDGEMENTS

REFERENCES

Allasia D., Bock L.E., Vasconcelos J., Pinto L.C., Tassi R., Minetto B., Persch C.G., and Pachaly R.L. Experimental study of geysering in an upstream vertical shaft. *Water*, 15:1740, 2023.

Greenshields C. and Weller H. *Notes on Computational Fuid Dynamics: General Principles*, volume I. CFD Direct Limited, 2022.

Guo Q. and Song C.C.S. Dropshaft hydrodynamics under transient conditions. *Journal of Hydraulic Engineering*, 117:1042–1055, 1991.

Menter F.R. Two-equation eddy-viscosity turbulence models for engineering appllications. *AIAA Journal*, 32:1598–7656–15924–1–RV1605, 1994.

Muller K., Wang J., and Vasconcelos J. Water displacement in shafts and geysering created by uncontrolled air pocket releases. *Journal of Hydraulic Engineering*, 143:04017043, 2017.

Vasconcelos J.G. and Wright S.J. Geysering generated by large air pockets released through water-filled ventilation shafts. *Journal of Hydraulic Engineering*, 137:543–555, 2011.

Wright S.J., Bosma C.D., and Lopez-Cantu T. Hydrologic design standards insufficient due to large increases in frequency of rainfall extremes. *Geophysical Research Letters*, 46:8144–8153, 2019.